

Neutron degeneracy and plasma physics effects on radiative neutron captures in neutron star crust

P. S. Shternin,^{1,2,*} M. Beard,³ M. Wiescher,³ and D. G. Yakovlev^{4,2,5}

¹*Ioffe Physical-Technical Institute, Politekhnicheskaya 26, 194021 St.-Petersburg, Russia*

²*St.-Petersburg State Polytechnical University, Politekhnicheskaya 29, St.-Petersburg 195251, Russia*

³*Department of Physics and The Joint Institute for Nuclear Astrophysics,
University of Notre Dame, Notre Dame, Indiana 46556, USA*

⁴*Ioffe Physical-Technical Institute, Politekhnicheskaya 26, St.-Petersburg 194021, Russia*

⁵*Department of Physics & The Joint Institute for Nuclear Astrophysics,
University of Notre Dame, Notre Dame, Indiana 46556, USA*

(Dated: July 26, 2012)

We consider the astrophysical reaction rates for radiative neutron capture reactions (n, γ) in the crust of a neutron star. The presence of degenerate neutrons at high densities (mainly in the inner crust) can drastically affect the reaction rates. Standard rates assuming a Maxwell-Boltzmann distribution for neutrons can underestimate the rates by several orders of magnitude. We derive simple analytical expressions for reaction rates at a variety of conditions with account for neutron degeneracy. We also discuss the plasma effects on the outgoing radiative transition channel in neutron radiative capture reactions and show that these effects can also increase the reaction rates by a few orders of magnitude. In addition, using detailed balance, we analyze the effects of neutron degeneracy and plasma physics on reverse (γ, n) photodisintegration. We discuss the dependence of the reaction rates on temperature and neutron chemical potential and outline the efficiency of these reactions in the neutron star crust.

PACS numbers: 25.60.Tv, 26.60.Gj

I. INTRODUCTION

Nuclear reactions in the atmosphere and the crust of accreting neutron stars affect important observational manifestations such as X-ray bursts and superbursts (e.g., Refs. [1–4]) as well as deep crustal heating of neutron stars in X-ray transients (e.g., Refs. [4–7]). In the vicinity of the neutron drip density ($\rho \sim 4 \times 10^{11} \text{ g cm}^{-3}$ for the cold-catalyzed crust and $\rho \sim 6 \times 10^{11} \text{ g cm}^{-3}$ for the accreted crust [5]) and beyond in the inner crust the dense matter contains an increasing amount of free degenerate neutrons (see, e.g., Ref. [8]). Neutron capture and reverse reactions are important components of nuclear burning under these conditions [9]. Standard thermonuclear neutron capture rates, which are used in reaction network simulations of nucleosynthesis in stars or supernova explosions, are obtained (e.g., Ref. [10]), assuming the classical Maxwell-Boltzmann distribution of neutrons. However, free neutrons in the neutron star crust can be degenerate, in particular when the density exceeds the neutron drip point [8]. For instance, ground-state (cold-catalyzed) matter at $\rho = 6.2 \times 10^{12} \text{ g cm}^{-3}$ has a neutron Fermi energy of $\approx 2.6 \text{ MeV}$ [11]. Consequently neutron degeneracy needs to be taken into account for neutron capture rates under such conditions.

In addition, the dense stellar plasma of the neutron star crust strongly affects emission, absorption, and propagation of photons [12] and therefore modifies radiative capture and photodisintegration reactions, like (n, γ) and

(γ, n). Because of the high density, the electron plasma frequency ω_p can be of the order of or higher than characteristic frequencies of radiative transitions in nuclei. Under these conditions, well-defined elementary electromagnetic excitations (photons or plasmons) become either suppressed or forbidden (e.g., Ref. [13]) although radiative transitions are not suppressed because they can be realized by emission (or absorption) of excess energy to (from) the plasma as a collective system [12]. These plasma physics effects can be important since they may enhance the radiative transition strength.

In Sec. II we discuss the effects of neutron degeneracy on (n, γ) radiative neutron capture reactions in dense matter. In Sec. III we analyze plasma effects on the outgoing radiative transition channel of (n, γ) reactions. In Sec. IV we consider the same neutron degeneracy and plasma physics effects on inverse (γ, n) photodisintegration reactions. We discuss our results in Sec. V and summarize them in Sec. VI. For brevity, we use the units in which the Boltzmann constant $k_B = 1$.

II. REACTION RATES FOR DEGENERATE NEUTRONS

We start with the outline of the (n, γ) radiative capture rates in stellar environments (e.g., Ref. [10]). Let the cross section $\sigma_{ab}(E)$ refer to the reaction $X^{(a)} + n \rightarrow Y^{(b)} + \gamma$, where a and b label different energy levels of a target nucleus X and a resultant nucleus Y , respectively, and E is the center-of-mass energy of the reactants. In stellar matter at local thermodynamic equilibrium, the

* pshternin@gmail.com

total cross section $\sigma^*(E)$ of the reaction $X + n \rightarrow Y + \gamma$ includes neutron capture on the ground state and all thermally populated states,

$$\sigma^*(E) = \frac{\sum_a g_a \exp(-E_X^{(a)}/T) \sum_b \sigma_{ab}(E)}{\sum_a g_a \exp(-E_X^{(a)}/T)}, \quad (1)$$

where $E_X^{(a)}$ is the energy of level a and g_a is its statistical weight. The summation in the denominator normalizes the distribution of target nuclei over the energy levels a (gives the internal partition function of the target nucleus). Asterisk $*$ means that thermally excited nuclear levels in stellar matter are included.

The astrophysical reaction rate contains the average $\langle \sigma^* v \rangle$ of the total cross section with the energy distribution $f(E)$ of the interacting particles. For nonrelativistic reactants (considered in this paper) the collision energy is $E = \mu v^2/2$, where μ is the reduced mass (very close to the neutron mass m_n), and v is the relative velocity of a neutron with respect to nucleus at large separations. Then

$$\langle \sigma^* v \rangle = \sqrt{\frac{2}{\mu}} \frac{1}{\mathcal{N}} \int_0^\infty E \sigma^*(E) f(E) dE, \quad (2)$$

where \mathcal{N} is the normalization factor

$$\mathcal{N} = \int_0^\infty \sqrt{E} f(E) dE. \quad (3)$$

We call $\langle \sigma^* v \rangle$ [$\text{cm}^3 \text{s}^{-1}$] the reaction rate coefficient. The rate itself (for instance, per unit volume, $\text{cm}^{-3} \text{s}^{-1}$) is $n_X n_n \langle \sigma^* v \rangle$, where n_n and n_X are number densities of neutrons and reacting nuclei, respectively.

Astrophysical reaction rates at typical stellar temperatures are based on a Maxwell-Boltzmann distribution of the particles, $f_{\text{MB}}(E) = \exp(-E/T)$. At high densities in the neutron star crust, neutrons can become degenerate, which modifies the reaction rate. At these conditions the nuclei are not freely moving particles but are confined in a strongly coupled Coulomb liquid or a Coulomb crystal (e.g., Ref. [8]). Because the neutrons are much lighter than the nuclei, the energy distribution function $f(E)$ in Eq. (2) can be approximated by a Fermi-Dirac distribution $f_{\text{FD}}(E) = [1 + \exp((E - \mu_n)/T)]^{-1}$, where μ_n is the neutron chemical potential. In this approximation we neglect recoil effects and nucleus motion. In the inner crust of the neutron star the nuclei can be bulky and occupy a non-negligible fraction of volume [14]. Here we employ the model of a free neutron gas with local number density n_n which occupies the space between the nuclei. Though this model is rather accurate near the neutron drip point, it becomes less accurate at higher densities where free neutrons constitute a strongly interacting Fermi liquid [11].

Let the average $\langle \sigma^* v \rangle_{\text{MB}}$ be obtained with the Maxwell-Boltzmann distribution and $\langle \sigma^* v \rangle_{\text{FD}}$ be calculated with the Fermi-Dirac distribution. Many calculated

reaction rate coefficients $\langle \sigma^* v \rangle_{\text{MB}}$ for neutron capture reactions are available in the literature (e.g., Ref. [15] and references therein). In a neutron star crust $\langle \sigma^* v \rangle_{\text{FD}}$ depends on T and μ_n (or, equivalently, on T and n_n). For practical applications we introduce the ratio

$$R_n \equiv \frac{\langle \sigma^* v \rangle_{\text{FD}}}{\langle \sigma^* v \rangle_{\text{MB}}}. \quad (4)$$

These ratios are easier to calculate and approximate than $\langle \sigma^* v \rangle_{\text{FD}}$; the derivation of these ratios is the main subject of the present paper.

Generally, accurate calculations of $\langle \sigma^* v \rangle_{\text{FD}}$ and R_n require the cross sections $\sigma_{ab}(E)$ obtained from experiment or nuclear reaction codes. Detailed calculations of $\langle \sigma^* v \rangle_{\text{FD}}$ would be a valuable project for the future. Here we restrict ourselves to a simplified approach. It allows us to demonstrate the importance of the effects of neutron degeneracy and is sufficiently accurate for a wide range of temperatures and densities. First, we neglect the contribution of thermally excited states (setting thus $\sigma^*(E) = \sigma(E)$). This is a valid approach if the energy of the first excited level of the target nucleus is higher than the temperature in the neutron star crust ($T \lesssim 2 \times 10^9 \text{ K} \approx 0.2 \text{ MeV}$). For threshold (endothermic) reactions, it should also be higher than the reaction threshold E_0 . Second, we note that the reaction rates at low temperatures correspond to cross sections $\sigma(E)$, which are characterized by typical power-law behavior that we therefore adopt in our analysis:

$$\sigma(E) = \sigma_a (E - E_0)^\nu \quad \text{at } E_0 \leq E \lesssim E_{\text{max}}. \quad (5)$$

Here, ν is a power-law index, σ_a is a normalization constant, E_0 is a reaction threshold (with $E_0 = 0$ for exothermic reactions), and E_{max} is the maximum energy up to which the approximation (5) holds. We treat E_0 , σ_a , ν , and E_{max} as input parameters. For a given reaction, they can be adopted from a nuclear database or calculated using a nuclear reaction code. In our approximation, the factor R_n depends on T , μ_n , ν , and E_0 ; the parameter σ_a cancels out in the ratio (4); E_{max} is required to check the validity of the calculated R_n for given conditions.

The reaction rates are strongly affected by the neutron energy distribution. Typical energies of nondegenerate neutrons are $E \lesssim T$. In a strongly degenerate gas ($\mu_n \gg T$) the majority of neutrons belong to the Fermi sea and have much higher energies $T \ll E \lesssim \mu_n$. In this case, there is also a smaller (but non-negligible) amount of neutrons, with energies above μ_n : $\mu_n \lesssim E \lesssim \mu_n + T$. Their distribution $f_{\text{FD}}(E) \approx \exp((\mu_n - E)/T) = \exp(\mu_n/T) f_{\text{MB}}(E)$ is close to Maxwellian and represents the Maxwellian tail of the Fermi-Dirac distribution. In the following we demonstrate that these different energy ranges of $f_{\text{FD}}(E)$ correspond to different neutron capture regimes.

For all nuclear reactions shown in the paper we use the cross sections obtained with the statistical model Hauser-Feshbach (HF) code TALYS-1.2 [16]. Statistical

model theory [17] uses the concept of averaged transmission coefficients to describe the formation and subsequent decay of a compound nucleus formed after a projectile impinges on a target nucleus. In this scenario the reaction sequence for neutron capture becomes $X^{(a)} + n \rightarrow C^* \rightarrow Y^{(b)} + \gamma$, where C^* is a compound nucleus with many closely spaced energy levels (high level density). For the neutron star crust conditions the incident neutron has rather low energy and the primary reaction mechanism is dominated by compound formation. The partial cross section $\sigma_{ab}(E)$ in the HF model is written as the sum over levels c (specified by energy E_c , spin J , and parity π) of the compound nucleus

$$\sigma_{ab}(E) = \frac{\pi}{k^2} \sum_c \frac{g_c}{g_n g_a} \frac{\mathcal{T}_{n,a}^c \mathcal{T}_{\gamma,b}^c}{\mathcal{T}_{\text{tot}}^c}. \quad (6)$$

In this case, k is the wave number of an incident neutron, $\mathcal{T}_{n,a}^c$ and $\mathcal{T}_{\gamma,b}^c$ are partial transmission coefficients, and $\mathcal{T}_{\text{tot}}^c$ is the total transmission coefficient of the compound nucleus in a level c . The latter quantity, $\mathcal{T}_{\text{tot}}^c \equiv \sum_{o,b} \mathcal{T}_{o,b}^c$, gives the total width of the c level as the sum over all available outgoing reaction channels $o = n, \gamma$, etc. and over levels b of the final nucleus. Note, that the sum includes compound elastic scattering (when final states are the same as the initial ones).

The individual neutron transmission coefficient for

each allowed channel is obtained by solving the Schrödinger equation with an optical potential for the neutron-nucleus interaction. The γ -transmission coefficient is calculated for a giant dipole resonance (E1+M1) approximated by a single Lorentzian or by a combination of Lorentzians [18–20]. The sum of these contributions determines the γ -ray strength function. Both the neutron and γ -ray transmission coefficients must be calculated for all accessible states. In practice there is a huge number of levels, the vast majority of which are experimentally unexplored. For very neutron-rich nuclei near the drip line the level density may be much smaller and the applicability of the HF model may be questionable.

Other necessary ingredients for a HF calculation include the choice of level density, optical model, γ -ray strength function, and mass model to predict the reaction Q value. The reaction cross sections presented here do not include pre-equilibrium effects. The cross sections are calculated on the basis of Q values derived from the Hartree-Fock-Bogoliubov mass model HFB-17 [21]. The level densities are obtained from the microscopic model of Ref. [22], and the E1 γ -ray strength function is based on quasiparticle random-phase-approximation calculations, folded with a simple Lorentzian [23]. The neutron optical potential is supplied by the global parametrizations of Ref. [24].

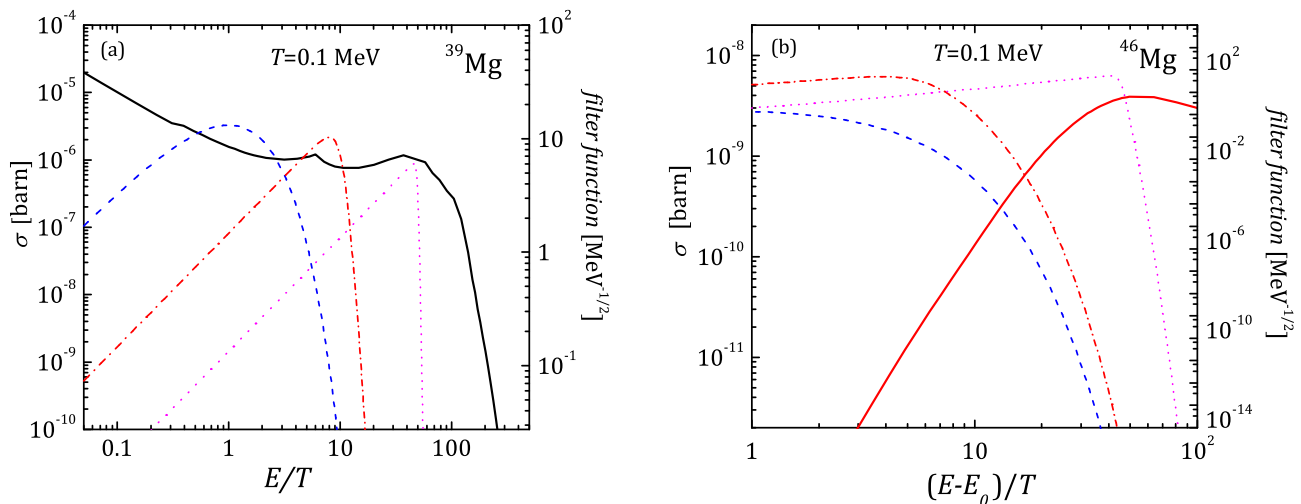


FIG. 1. Cross sections σ of neutron capture on ^{39}Mg (panel (a)) and ^{46}Mg (panel (b)) plotted (left vertical axis) in double logarithmic scale as a function of $(E - E_0)/T$ at $T = 0.1$ MeV. In both panels we show also (right vertical axis) the filter functions $Ef(E)/\mathcal{N}$ for the three cases: Maxwell-Boltzmann distribution (dashed lines) and Fermi-Dirac distribution with $\mu_n = 1$ MeV (dash-dotted lines) and $\mu_n = 5$ MeV (dotted lines). See text for details.

Figure 1 shows the reaction cross sections (left vertical

scales) for two neutron capture reactions, on ^{39}Mg (panel

(a)) and ^{46}Mg (panel (b)). The $^{39}\text{Mg}(n, \gamma)^{40}\text{Mg}$ reaction is exothermic ($E_0 = 0$), while the $^{46}\text{Mg}(n, \gamma)^{47}\text{Mg}$ is endothermic ($E_0 = 4.06$ MeV). For a better visualization of the approximation (5), $\sigma(E)$ is shown as a function of $(E - E_0)/T$ on a double logarithmic scale; the temperature is taken to be $T = 0.1$ MeV. The linear segments of the curves clearly indicate the power-law behavior of $\sigma(E)$ at low E . Power-law indices and maximum energies are $\nu = -0.6$ and $E_{\text{max}} \approx 0.1$ MeV for neutron capture on ^{39}Mg ; $\nu = 3.5$ and $E_{\text{max}} \approx 6$ MeV for neutron capture on ^{46}Mg . This power-law behavior at low energies is typical for (n, γ) reactions. Figure 1 also shows (right vertical scales) the so-called filter functions $E f(E)/\mathcal{N}$, which enter the integrand of (2) along with $\sigma^*(E)$. The dashed lines in both panels correspond to the Maxwell-Boltzmann distributions of neutrons. We see that the power-law approximation is sufficient for calculating $\langle \sigma v \rangle_{\text{MB}}$ in both cases (at $T = 0.1$ MeV). The dash-dotted and dotted lines in Fig. 1 represent the Fermi-Dirac distribution with $\mu_n = 1$ MeV and 5 MeV, respectively. We see that for $\mu_n = 1$ MeV and the ^{46}Mg target the power-law approximation is definitely valid, while for $\mu_n = 5$ MeV it is less accurate. For neutron capture on the ^{39}Mg nucleus, the power-law approximation is inaccurate at both values of μ_n .

It is easy to see that the power-law approximation (5) is valid as long as $\max(E_0, \mu_n) + T \lesssim E_{\text{max}}$. In this approximation, the factor R_n in Eq. (4) is calculated analytically. By introducing dimensionless parameters $y = \mu_n/T$ and $x_0 = E_0/T$, we obtain,

$$R_n = \frac{\exp x_0}{x_0 + \nu + 1} \frac{(\nu + 1)\mathcal{F}_{\nu+1}(y - x_0) + x_0\mathcal{F}_{\nu}(y - x_0)}{\mathcal{F}_{1/2}(y)}, \quad (7)$$

where $\mathcal{F}_{\nu}(y)$ is a Fermi-Dirac integral

$$\mathcal{F}_{\nu}(y) = \frac{1}{\Gamma(\nu + 1)} \int_0^{\infty} \frac{x^{\nu} dx}{1 + \exp(x - y)}, \quad (8)$$

and $\Gamma(\nu + 1)$ is the Euler gamma-function.

Equation (7) is the main result of our consideration. We expect that this factor is sufficient to correct the reaction rate for neutron degeneracy in many cases of practical importance. Let us analyze the limiting cases. For this purpose we use asymptotes of the Fermi-Dirac integrals given in the Appendix.

First consider a threshold reaction with typical neutron energies well below the threshold. In this case $x_0 - y \gg 1$ ($E_0 - \mu_n \gg T$), and Eq. (7) becomes

$$R_n = \frac{\exp y}{\mathcal{F}_{1/2}(y)}. \quad (9)$$

If, in addition, neutrons are strongly degenerate ($y \gg 1$), Eq. (9) is further simplified,

$$R_n = \frac{3\sqrt{\pi}}{4} y^{-3/2} \exp y. \quad (10)$$

The factor R_n in Eqs. (9) and (10) becomes a function of only one parameter, $y = \mu_n/T$; it is independent of ν . This indicates that Eqs. (9) and (10) are valid for any cross sections $\sigma(E)$ of threshold reactions, not only for ones with power-law behavior. Indeed, in the limit $x_0 - y \gg 1$ the majority of neutrons have energies $E < E_0$; these neutrons cannot overcome the reaction threshold and cannot be captured by nuclei. The reaction proceeds owing to a small amount of high-energy (suprathermal) neutrons with $E > E_0$. Recall that for any neutron degeneracy, their distribution function in Eq. (2) is actually Maxwellian, $f_{\text{FD}}(E) \approx \exp(\mu_n/T) f_{\text{MB}}(E)$. Then the cross sections in the nominator and denominator of Eq. (4) are integrated with the same function $f_{\text{MB}}(E)$; equal integrals for any $\sigma(E)$ cancel out and do not affect the ratio R_n .

The ratio R_n in Eq. (10) shows a sharp exponential y -dependence at strong neutron degeneracy. This means that neutron degeneracy exponentially enhances the rates of threshold reactions (by increasing the amount of high-energy neutrons).

Another limiting case is the one of an (endo- or exothermic) reaction with strongly degenerate neutrons whose typical energies are above the reaction threshold. In this limit $y - x_0 \gg 1$ ($\mu_n - E_0 \gg T$), the reaction is driven by numerous energetic Fermi-sea neutrons and becomes fast, with

$$R_n = \frac{3\sqrt{\pi} \exp x_0}{4\Gamma(\nu + 3)} \frac{(y - x_0)^{\nu+1}}{y^{3/2}} \frac{x_0 + (\nu + 1)y}{x_0 + \nu + 1}. \quad (11)$$

In particular, for a threshold reaction with strongly degenerate neutrons at $E_0 \gg T$ and $\mu_n \gg T$, R_n is given by Eq. (10) for $E_0 - \mu_n \gg T$ and by Eq. (11) for $\mu_n - E_0 \gg T$. These two asymptotes nearly match each other at $|\mu_n - E_0| \sim T$ providing an accurate description of R_n in a wide range of μ_n except for the narrow interval $|\mu_n - E_0| \lesssim T$ that should be described by Eq. (7).

At $\mu_n > E_0$ the dependence of R_n on the neutron degeneracy parameter y is much weaker than at $\mu_n < E_0$. In the range of $T \ll \mu_n - E_0 \ll E_0$, Eq. (11) can be simplified by setting $y = x_0$ everywhere but in $(y - x_0)^{\nu+1}$; this gives $R_n \propto (\mu_n - E_0)^{\nu+1}$. For higher $\mu_n \gg E_0$ we have $R_n \propto \mu_n^{\nu+1/2}$.

In order to calculate R_n in intermediate cases from Eq. (7), accurate expressions for Fermi-Dirac integrals are necessary. These integrals have been extensively studied in the literature, especially in the field of semiconductor physics and astrophysics (e.g., Ref. [25, 26] and references therein). There are several very accurate approximations for particular integer and half-integer values of ν . An analytic approximation that can be used for any ν in the range $-1 < \nu < 4$ was constructed by Aymerich-Humet et al. [27]. It accurately reproduces the limits of $y \rightarrow \pm\infty$, and its relative error at $-1/2 < \nu < 5/2$ does not exceed 1.2%. For convenience, we present this approximation in the Appendix.

III. PLASMA EFFECTS

In addition to the effects of neutron degeneracy, the rates of (n, γ) reactions in dense matter are influenced by electron plasma effects. Under typical conditions in the neutron star crust, the electrons behave as weakly interacting, strongly degenerate and ultra-relativistic particles [8]. The importance of plasma effects is characterized by the electron plasma frequency $\omega_p = \sqrt{4\pi e^2 n_e / m_e^*}$, where e is the electron charge, n_e is the electron number density, and $m_e^* = \mu_e / c^2$ is the effective electron mass at the Fermi surface (μ_e being the electron chemical potential). The plasma effects modify the radiative transition in the exit channel. The plasma effects are strong when the frequency ω of a radiative transition becomes comparable to ω_p . In particular, no well-defined electromagnetic excitations (photons or plasmons) can propagate at $\omega < \omega_p$ (e.g., Ref. [13]). In this case the radiative transition cannot occur through the emission of a real photon or plasmon. However, it can occur through a direct transfer of the excess energy $\hbar\omega$ to plasma electrons via collision-free collective electromagnetic interactions. For a degenerate electron plasma in the neutron star crust, this effect was considered in Ref. [12]. It does not suppress but rather enhances radiative transitions at $\omega \lesssim \omega_p$. The enhancement factor $\mathcal{R}_\gamma(\omega)$ depends on the radiative transition type (electric or magnetic), on the transition multiplicity $\ell = 1, 2, \dots$, and on the ω/ω_p ratio. In the low-frequency limit, $\omega \ll \omega_p$, this factor behaves as $\mathcal{R}_\gamma(\omega) \sim (\omega_p/\omega)^{2\ell}$, while at $\omega \gg \omega_p$ one has $\mathcal{R}_\gamma(\omega) \rightarrow 1$, meaning that the plasma effects become less important and the standard regime of emission of real photons is restored.

The plasma effects modify the reaction cross section $\sigma(E)$ and the reaction rate coefficient $\langle\sigma v\rangle$. In analogy with Eq. (4) we can formally introduce the total correction factor

$$R_{n,\text{pl}} = \frac{\langle\sigma_{\text{pl}} v\rangle_{\text{FD}}}{\langle\sigma v\rangle_{\text{MB}}}, \quad (12)$$

which takes into account both neutron degeneracy and plasma effects; $\sigma(E)$ and $\sigma_{\text{pl}}(E)$ are the cross sections excluding and including the plasma effects, respectively. It is convenient to write

$$R_{n,\text{pl}} = R_n R_{\text{pl}}, \quad (13)$$

where R_n takes into account neutron degeneracy alone as discussed in Sec. II, and R_{pl} accounts for plasma effects (in the presence of neutron degeneracy).

The inclusion of plasma effects in (n, γ) reaction rates is not straightforward. As discussed in Sec. II, the rates of interest are usually calculated [10] in the framework of the HF statistical model [17]. The radiative transition coefficients need to be modified in the numerator and denominator of Eq. (6). The problem is further complicated by summing over thermally excited nuclear levels b in Eq. (1). For different levels b the energy and type

of radiative transition can be different (implying different plasma modifications). A correct inclusion of the plasma effects is therefore a complicated computational project, which is beyond the scope of our paper. Here, we present a simplified approach which demonstrates the importance of the plasma effects. It is based on the assumption that the radiative transmission coefficients \mathcal{T}_γ are much smaller than other contributions to the total transmission coefficient \mathcal{T}_{tot} in Eq. (6). In that case the total transmission coefficient \mathcal{T}_{tot} is independent of the plasma effects. The second assumption is that the radiative exit channel is represented by a single E1 radiative transition to the ground state, so that no summation over excited states b is required.

These requirements are realized for threshold (n, γ) reactions involving degenerate neutrons where μ_n is below or slightly above E_0 . In this case the typical energy of interacting neutrons is not much higher than E_0 , which reduces the radiative decay of the compound states to a single (not multiple) low-energy radiative transition.

Under these assumptions we can describe the plasma effects by multiplying the neutron capture cross section $\sigma(E)$ by the factor $\mathcal{R}_{\gamma\text{e1}}(\omega)$, with $\hbar\omega = E - E_0$, which describes the enhancement of the radiative transition by the plasma effects. The latter factor was calculated in Ref. [12] and fitted by a simple analytical expression (Eq. (33) in [12]) with an error of about 1%. The modified cross section must be integrated over E to obtain the reaction rate. To simplify the integration we suggest using the approximation

$$\mathcal{R}_{\gamma\text{e1}}(\omega) \approx 1 + 3.03 \left(\frac{\omega_p}{\omega} \right)^2. \quad (14)$$

Although it is rather crude at $\omega \sim \omega_p$, with the maximum error 17% at $\omega = \omega_p$, it reproduces the correct asymptotic behavior for $\omega \gg \omega_p$ and $\omega \ll \omega_p$. The deviation does not exceed 5% outside the region of $0.6 < \omega/\omega_p < 1.03$. The advantage of using Eq. (14) is that it allows an analytic integration of the correction to the reaction rate in the same power-law approximation for the cross section as used in Sec. II. Because $\mathcal{R}_{\gamma\text{e1}}(\omega)$ is integrated, the approximation errors cancel out, leaving us with a rather accurate result. The correction factor (12) to the reaction rate including both neutron degeneracy and electron plasma effects now becomes

$$R_{n,\text{pl}} = \frac{3.03}{\nu(\nu-1)} \left(\frac{\hbar\omega_p}{T} \right)^2 \frac{x_0 + \nu - 1}{x_0 + \nu + 1} R_n^{(\nu-2)} + R_n^{(\nu)}. \quad (15)$$

Here, $R_n^{(\nu)}$ is the factor given by Eq. (7) for a power-law index ν .

In the limit $E_0 - \mu_n \gg T$ for a threshold reaction with $E_0 \gg T$, the expression (15) is further simplified. Introducing the correction factor R_{pl} due to the plasma effects in accordance with Eq. (13), we have

$$R_{\text{pl}} = 1 + \frac{3.03}{\nu(\nu-1)} \left(\frac{\hbar\omega_p}{T} \right)^2. \quad (16)$$

In this limit, in addition to a strong exponential enhancement of the reaction rate due to neutron degeneracy (Sec. II), there is a smaller but significant plasma enhancement. In the opposite limit of $\mu_n - E_0 \gg T$ (but still for a single radiative transition) we obtain

$$R_{\text{pl}} = 1 + 3.03 \frac{(\nu+2)(\nu+1)}{\nu(\nu-1)} \left(\frac{\omega_p}{\omega} \right)^2 \frac{E_0 + (\nu-1)\mu_n}{E_0 + (\nu+1)\mu_n}. \quad (17)$$

This factor is temperature independent because the typical transition energy is now nearly fixed by μ_n and E_0 , $\hbar\omega \approx \mu_n - E_0$.

IV. RATES OF INVERSE REACTIONS

If the rate of a forward $X(n, \gamma)Y$ reaction is known, then the rate for an inverse reaction $Y(\gamma, n)X$ can be determined from the detailed balance principle,

$$n_X^{(\text{eq})} n_n^{(\text{eq})} \langle \sigma v \rangle = n_Y^{(\text{eq})} \lambda_\gamma, \quad (18)$$

where $n_X^{(\text{eq})}$, $n_Y^{(\text{eq})}$, and $n_n^{(\text{eq})}$ are number densities of nuclei X , Y , and neutrons, respectively, in statistical equilibrium between forward and inverse reactions. λ_γ [s^{-1}] specifies the rate of the inverse (photodisintegration) reaction (which is $n_Y \lambda_\gamma$, $\text{cm}^{-3} \text{s}^{-1}$). Usually, this reaction involves only photons γ but in our case it also can involve more complicated excitations associated with the electromagnetic field and plasma electrons (Sec. III), which are assumed to be in thermal equilibrium; their effective number density is included in λ_γ . The equilibrium number densities of the nuclei should satisfy the condition of chemical equilibrium

$$\mu_X + \mu_n = \mu_Y, \quad (19)$$

where μ_X and μ_Y are the chemical potentials of the nuclei X and Y , respectively. Traditionally one assumes ideal nondegenerate gas conditions for the nuclei and neutrons in order to relate their equilibrium number densities and chemical potentials. In this approximation Eq. (18) yields the well-known relation

$$\lambda_\gamma = \left(\frac{A_X m_n T}{2\pi \hbar^2 A_Y} \right)^{3/2} \frac{2\mathcal{Z}_X}{\mathcal{Z}_Y} \exp\left(-\frac{Q}{T}\right) \langle \sigma v \rangle_{\text{MB}}, \quad (20)$$

where A_X and $A_Y = A_X + 1$ are mass numbers of nuclei X and Y , respectively, while \mathcal{Z}_X and \mathcal{Z}_Y are their individual internal partition functions

$$\mathcal{Z}_X = \sum_a g_a \exp\left(-\frac{E_X^{(a)}}{T}\right). \quad (21)$$

The corresponding function for the neutrons is $\mathcal{Z}_n = 2$.

Now we should modify Eq. (20) to account for neutron degeneracy and strong Coulomb coupling of the nuclei.

Strong Coulomb coupling prevents treating the plasma of atomic nuclei as an ideal gas (it becomes Coulomb liquid or crystal; e.g., Ref. [8]). A strongly coupled multi-component plasma of charged particles satisfies (to a very high accuracy) the linear mixing rule according to which the main Coulomb thermodynamic quantities (like mean Coulomb energy, etc.) can be presented as sums of quantities for individual ions. Coulomb coupling of an individual atomic nucleus $X = (A_X, Z_X)$ in this plasma is described by the parameter $\Gamma_X = Z_X^2 e^2 / (a_X T)$, where a_X is the ion sphere radius defined as $a_X = [3Z_X / (4\pi n_e)]^{1/3}$. This allows one to treat a strongly coupled system of atomic nuclei as an ensemble of weakly interacting ion spheres. This approximation is well known in the physics of strongly coupled Coulomb plasmas [8]. In this case Eq. (20) remains the same but the internal partition function for each nucleus has to be multiplied by its individual Coulomb partition function $\mathcal{Z}_X^{(C)}$. A function $\mathcal{Z}_X^{(C)}$ depends only on one parameter, Γ_X , which, in turn, is determined by the nuclear charge number Z_X . Because in our case $Z_X = Z_Y$, we have $\mathcal{Z}_X^{(C)} = \mathcal{Z}_Y^{(C)}$, and the Coulomb corrections for the nuclei X and Y compensate for each other in Eq. (20).

Neutron degeneracy can be included in Eq. (20) by implying the correct relation between the neutron number density and its chemical potential. It is easy to show that for this purpose it is sufficient to multiply the right-hand side of Eq. (20) by

$$R_{\text{rvs}} = \exp(-y) \mathcal{F}_{1/2}(y). \quad (22)$$

The ratio of the photodisintegration rates for the Fermi-Dirac and the Maxwell-Boltzmann distributions of neutrons then becomes

$$\frac{\langle \lambda_\gamma \rangle_{\text{FD}}}{\langle \lambda_\gamma \rangle_{\text{MB}}} \equiv R_\lambda = R_{\text{rvs}} R_n. \quad (23)$$

If plasma effects are included, then R_n must be replaced by $R_{n,\text{pl}}$.

Various asymptotes for R_λ are readily obtained from those for R_n , Eqs. (9)–(11). In particular, for the case of a threshold neutron capture reaction with the neutron chemical potential well under the threshold, $E_0 - \mu_n \gg T$, we obtain (neglecting plasma effects) $R_\lambda = 1$ for any dependence of σ on E . The inverse reaction is not affected by neutron degeneracy which is quite natural. The effect of neutron degeneracy on an (γ, n) reaction consists of Pauli blocking of the emitted neutrons. However, in our case these neutrons have energies $E = Q + \hbar\omega \gg \mu_n$, above the Fermi level, where the blocking does not occur.

In the opposite limit, $\mu_n - E_0 \gg T$, the neutrons, emitted in the reverse reaction, have low energies and are strongly blocked by the Fermi sea neutrons; this exponentially suppresses the inverse reaction rate:

$$R_\lambda = \frac{(y - x_0)^{\nu+1} [x_0 + (\nu+1)y]}{(x_0 + \nu + 1) \Gamma(\nu+3)} \exp(x_0 - y). \quad (24)$$

Note that recently Mathews et al. [28] suggested modifying the detailed balance equation (20) by taking into account the quantum corrections due to induced photon effects in the photodisintegration rate coefficient λ_γ . They point out that while calculating λ_γ one usually employs the Maxwellian distribution of photons instead of the Planck distribution $f_{\text{Pl}} = (\exp(E_\gamma/T) - 1)^{-1}$. Using the Planck distribution, they corrected λ_γ and concluded that one should also correct the detailed-balance ratio $\lambda_\gamma / \langle \sigma v \rangle_{\text{MB}}$. However, in this latter conclusion the authors erroneously neglected the same corrections in the rate coefficient $\langle \sigma v \rangle_{\text{MB}}$ of the forward reaction. Specifically, they did not include an extra factor $(1 + f_{\text{Pl}}(E_\gamma))$ (with $E_\gamma = E + Q$) under the integral in their Eq. (6) (similar to Eq. (2) in the present paper) to account for the induced emission. If that factor would have been introduced, the detailed balance ratio would be naturally unaffected by quantum corrections. In our analysis we neglect such corrections in both forward and reverse reaction rates, because they are generally small [28].

V. DISCUSSION

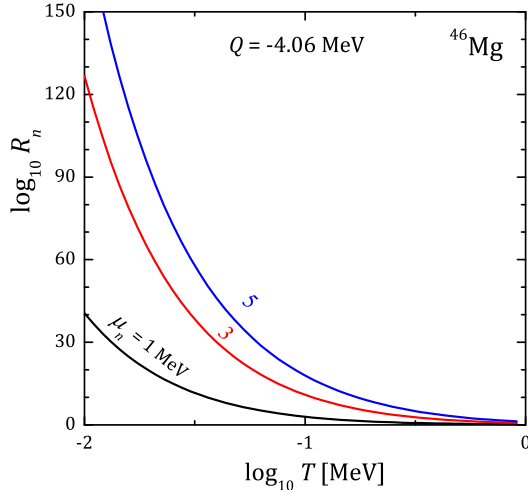


FIG. 2. Factor R_n for the $^{46}\text{Mg}(n, \gamma)^{47}\text{Mg}$ reaction as a function of temperature for $\mu_n = 1, 3$, and 5 MeV.

Let us illustrate the obtained results. First consider the effects of neutron degeneracy on threshold reactions neglecting plasma physics effects. Figure 2 shows R_n as a function of T for the $^{46}\text{Mg}(n, \gamma)^{47}\text{Mg}$ reaction at $\mu_n = 1, 3$, and 5 MeV. This reaction has a rather high threshold, $E_0 = 4.06$ MeV. We see a strong increase of the reaction rate with growing μ_n . For $\mu_n = 1$ and 3 MeV the factor R_n is well described with the power-law approximation by Eq. (9). For $\mu_n = 5$ MeV the difference to the power-law approximation becomes noticeable, but not on the logarithmic scale of Fig. 2.

To illustrate the possible deviations from the power-law approximation, in Fig. 3 we plot R_n versus μ_n at

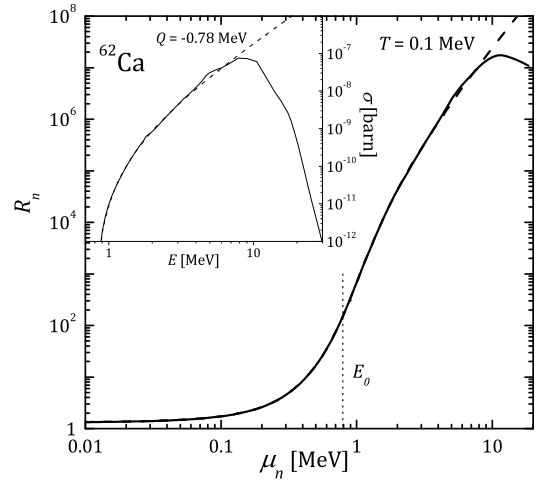


FIG. 3. Factor R_n for the $^{62}\text{Ca}(n, \gamma)^{63}\text{Ca}$ reaction as a function of μ_n at $T = 0.1$ MeV. Vertical dotted line indicates the reaction threshold. The inset shows the reaction cross section. Dashed lines in the figure and inset refer to the power-law approximation.

$T = 0.1$ MeV (the main figure) and $\sigma(E)$ (the inset) for the $^{62}\text{Ca}(n, \gamma)^{63}\text{Ca}$ reaction ($E_0 = -Q = 0.78$ MeV). The solid lines are obtained by numerical calculations, while the dashed lines are the results of the power-law approximation. It can be seen that the latter approximation accurately describes $\sigma(E)$ up to $E_{\text{max}} \approx 10$ MeV. Accordingly, Eq. (7) closely reproduces the dependence of R_n on μ_n at $\mu_n \lesssim 10$ MeV; the exponential asymptote (10) is valid at $\mu_n \lesssim 1.5$ MeV; the power-law asymptote (11) works well at $1.5 \lesssim \mu_n \lesssim 10$ MeV. At $\mu_n \gtrsim 10$ MeV the power-law approximation becomes inaccurate because at such μ_n the reaction rate is affected by the high-energy segment of $\sigma(E)$ where the power-law is invalid.

The situation is different with exothermic reactions. Figure 4 shows the calculated factor R_n for the $^{39}\text{Mg}(n, \gamma)^{40}\text{Mg}$ reaction. The reaction is exothermic ($E_0 = 0$, $Q = 1.4$ MeV); its cross section is plotted in the left panel of Fig. 1. The solid, dashed, and dot-dashed lines in Fig. 4 are calculated for $\mu_n = 0.2, 1$, and 5 MeV, respectively. Thick lines are obtained by integration of numerically calculated cross sections; thin lines are obtained using the power-law approximation. We see that the effect of neutron degeneracy is much weaker than for threshold reactions; the factor R_n stays ~ 1 . Notice that for $\mu_n = 0.2$ and 1 MeV the Fermi-Dirac averaged rate is smaller than the Maxwell-Boltzmann rate ($R_n < 1$). The power-law approximation breaks down even for small values of μ_n ($\sigma(E)$ starts to deviate from power-law at $E \lesssim 0.2$ MeV, see Fig. 1).

Now let us discuss the impact of plasma effects on neutron capture reactions starting with the threshold reactions. In all cases the plasma effects cause an additional enhancement of the reaction rates. Figure 5 gives R_{pl} for the $^{38}\text{Mg}(n, \gamma)^{39}\text{Mg}$ reaction as a function of μ_n at the

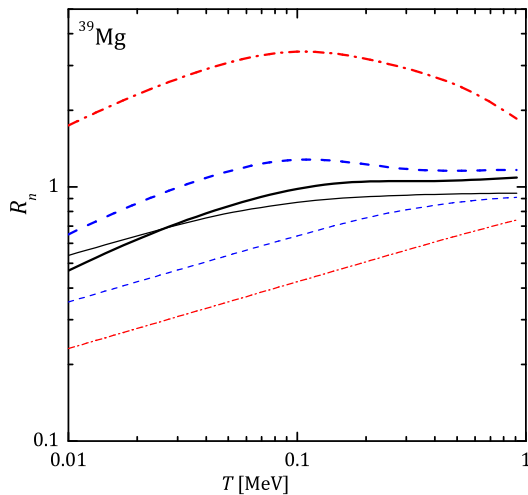


FIG. 4. Factor R_n for the $^{39}\text{Mg}(n, \gamma)^{40}\text{Mg}$ reaction as a function of temperature at $\mu_n = 0.2, 1$, and 5 MeV (solid, dashed, and dot-dashed lines, respectively). Shown are results of numerical integration of calculated cross section $\sigma(E)$ (thick lines) and results of the power-law approximation (thin lines).

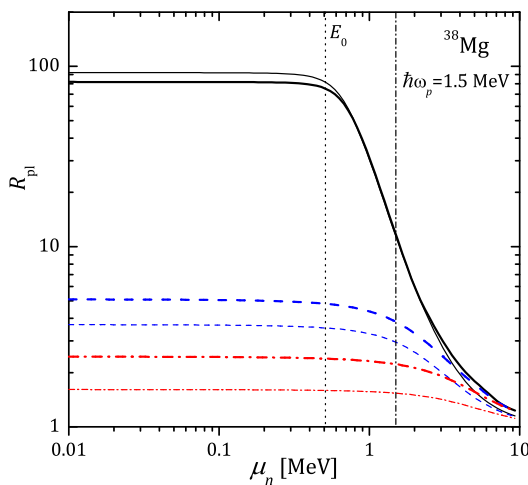


FIG. 5. Factor R_{pl} vs μ_n for the $^{38}\text{Mg}(n, \gamma)^{39}\text{Mg}$ reaction in matter with the electron plasma frequency $\hbar\omega_p = 1.5$ MeV. Solid, dashed, and dash-dotted curves are plotted for $T = 0.1, 0.5$, and 1 MeV, respectively. Thick curves are obtained using computed $\sigma(E)$ and accurate approximation of $\mathcal{R}_{\gamma e1}(\omega)$; thin curves represent the approximation (15). Vertical dotted and dash-dotted lines indicate the reaction threshold and plasma frequency, respectively.

electron plasma frequency $\hbar\omega_p = 1.5$ MeV. The curves are plotted for $T = 0.1$ (solid lines), 0.5 (dashed lines), and 1 MeV (dash-dotted lines). Thick curves are calculated with numerically determined cross section and an accurate plasma enhancement factor $\mathcal{R}_{\gamma e1}(\omega)$ from Ref. [12]. Thin curves are given by simplified Eq. (15). All curves change their behavior when μ_n reaches the reaction threshold $E_0 = -Q = 0.5$ MeV. For $\mu_n < E_0$,

the typical energy released in the radiative transition is $\hbar\omega \sim T$, while at $\mu_n > E_0$ it is $\hbar\omega \approx \mu_n - E_0$. Therefore, at $\mu_n < E_0$ the factor R_{pl} is mostly independent of μ_n , while at $\mu_n > E_0$ it is independent of T (cf. Eqs. (16) and (17)). A significant plasma enhancement can be observed at $\mu_n < E_0$. It is most visible for the solid curves (in those segments where T and μ_n are smaller than ω_p). The plasma enhancement is expected to be especially pronounced in those reactions which occur in dense plasma and are accompanied by small radiative energy release.

The difference between the thick (more accurate) and thin (less accurate) lines in Fig. 5 is small for $T = 0.1$ MeV but is higher for $T = 0.5$ and 1 MeV. This is solely due to the breakdown of the power-law approximation of $\sigma(E)$ for the $^{38}\text{Mg}(n, \gamma)^{39}\text{Mg}$ reaction at $E \gtrsim 1.5$ MeV. We have checked that using Eq. (14) instead of the more accurate approximation to $\mathcal{R}_{\gamma e1}(\omega)$ from Ref. [12] does not significantly change the results.

For exothermic reactions the simple model used in Sec. III is generally inapplicable. We expect that plasma effects on these reactions give $R_{\text{pl}} \sim 1$.

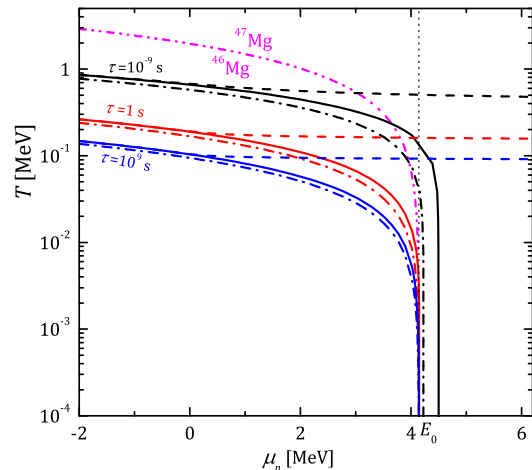


FIG. 6. Lines of constant effective times $\tau = 10^{-9}, 1, 10^9$ s of ^{46}Mg burning in the $^{46}\text{Mg}(n, \gamma)^{47}\text{Mg}$ reaction on the T - μ_n plane. We present calculations using the Maxwell-Boltzmann neutron capture rate (dashed lines), the rate corrected for neutron degeneracy (solid lines), and the rate corrected for degeneracy and plasma physics effects (dash-dotted lines). Vertical dotted line positions the reaction threshold $E_0 = 4.06$ MeV. The double-dot-dashed line corresponds to equal amounts of ^{46}Mg and ^{47}Mg nuclei, assuming statistical equilibrium with respect to neutron capture and emission reactions.

Finally, in order to illustrate the efficiency of neutron captures, in Fig. 6 we plot the lines of constant characteristic burning times τ of ^{46}Mg nuclei in the $^{46}\text{Mg}(n, \gamma)^{47}\text{Mg}$ reaction. The plot is made in the T - μ_n plane for the three values of $\tau = 10^{-9}, 1, 10^9$ s. The characteristic burning time is defined as

$$\tau^{-1} = n_n \langle \sigma v \rangle. \quad (25)$$

In the region above and to the right of each line burning is faster than on the line (τ is smaller); in the region below and to the left burning is slower. Lines of different types are calculated using different reaction rates. The dashed lines are for non-degenerate neutrons, the solid lines take into account neutron degeneracy, and the dot-dashed lines take into account neutron degeneracy and plasma effects (assuming $\hbar\omega_p = 1.5$ MeV). Neutrons are essentially non-degenerate in the region of $\mu_n \lesssim 0$ (in the left part of the $\mu_n - T$ plane). They are strongly degenerate in the region of $\mu_n \gtrsim T$.

As long as neutrons are non-degenerate, the solid and dashed lines naturally coincide. When neutron degeneracy sets in, it intensifies neutron captures. Then the solid lines (in sharp contrast with the dashed ones) bend and become nearly vertical. In this regime neutron degeneracy is vitally important. The most remarkable effect occurs in the vicinity of the threshold ($\mu_n = E_0 = 4.06$ MeV, shown by the dotted vertical line). We see that the solid lines drop off to zero temperature almost immediately after μ_n exceeds the reaction threshold. In this case the reaction is driven by the Fermi sea of degenerate neutrons and becomes extremely fast.

The purpose of Fig. 6 is primarily to illustrate the efficiency of the $^{46}\text{Mg} \rightarrow ^{47}\text{Mg}$ transformation with respect to neutron capture, neglecting other reactions (reverse reaction, beta captures, and fusion reactions). Its main and natural result is that ^{46}Mg cannot survive for a long time against neutron capture when μ_n exceeds E_0 .

According to Fig. 6, the $^{46}\text{Mg} \rightarrow ^{47}\text{Mg}$ reaction actually occurs in a narrow strip on the $T - \mu_n$ plane that is confined between the lines $\tau = 10^{-9}$ s and $\tau = 10^9$ s. Below and to the left of the $\tau = 10^9$ line, τ is very large; there will be plenty of ^{46}Mg nuclei which are very inefficient neutron absorbers. Above and to the right of the $\tau = 10^{-9}$ s line, τ is extremely short; all ^{46}Mg nuclei are transformed into ^{47}Mg . The shape of this “burning” strip is similar to that for fusion reactions; see, for instance, Fig. 4 of Ref. [29], which gives the strip for the $^{12}\text{C} + ^{12}\text{C}$ fusion reaction in the $T - \rho$ plane. The bend of the carbon burning $\tau = \text{const}$ lines at high densities ρ is produced due to the transition from thermonuclear carbon fusion to pycnonuclear one. It greatly resembles the bend of the $\tau = \text{const}$ curves with the growth of μ_n due to the effects of neutron degeneracy in our Fig. 6.

In addition, the double-dot-dashed curve in Fig. 6 is the line representing equal amounts of ^{46}Mg and ^{47}Mg nuclei ($n_X^{(\text{eq})} = n_Y^{(\text{eq})}$), assuming statistical equilibrium with respect to the neutron capture and reverse reactions. In statistical equilibrium, the matter (in our simplified model) would mainly contain ^{46}Mg nuclei below this line and ^{47}Mg nuclei above this line.

VI. CONCLUSIONS

We have considered neutron captures (n, γ) in dense stellar matter, taking into account the effects of neutron

degeneracy and plasma physics. The effects of neutron degeneracy increase the amount of high-energy neutrons and mainly enhance the reaction rates; plasma physics effect enhance the radiative transition in the outgoing channel and enhance the reaction rates as well.

The effects of neutron degeneracy on neutron capture reaction rates can be quantified by introducing the ratio R_n , Eq. (4), of rates calculated for given conditions to those for non-degenerate neutrons. We have described this ratio by a simple analytic expression (7) assuming the power-law energy dependence of the reaction cross section (5) at energies that are not too high. The derived expression (7) seems sufficient for many applications. Furthermore, approximating $\sigma(E)$ by a power-law function (5), one also obtains the power-law index ν and the maximum energy E_{max} to which the power-law approximation of $\sigma(E)$ is valid. E_0 and ν are needed in Eq. (7), while E_{max} controls the validity of Eq. (7).

Our conclusions are as follows:

1. Neutron degeneracy can significantly affect (n, γ) reactions in deep neutron star crust (Sec. II). In many cases the effects of neutron degeneracy are well described by the factor R_n given by Eq. (7). For threshold reactions, strong neutron degeneracy enhances the reaction rate by many orders of magnitude.
2. Plasma physics effects can additionally enhance (n, γ) rates (Sec. III), that is described by the factor R_{pl} . These effects are less dramatic but can reach a few orders of magnitude.

Furthermore, in Sec. IV we have used the detailed balance principle and calculated the rates of inverse (γ, n) reactions taking into account neutron degeneracy and plasma effects. Finally, in Sec. V we discussed the efficiency of (n, γ) reactions in a neutron star crust, with the conclusion that neutron degeneracy can be most important.

Finally it should be noted that free degenerate neutrons in a neutron star crust can be in a superfluid state. Critical temperature T_{cn} for the appearance of neutron superfluidity is very model dependent. Numerous calculations using different techniques (e.g., Ref. [30]) give density-dependent $T_{\text{cn}}(\rho)$ with maximum values ranging from $\sim 0.2 - 0.3$ MeV to ~ 2 MeV, indicating that superfluidity is most likely. Superfluidity produces a gap in the energy spectrum of neutrons near the Fermi level and modifies matrix elements of neutron capture reactions. Both effects on neutron captures are not explored but may strongly modify the reaction rates.

Our consideration of neutron degeneracy and plasma effects on neutron capture rates is simplified. A more rigorous (and complicated) analysis of these effects (including also neutron superfluidity) would be desirable. It would be instructive to perform self-consistent calculations of the structure of atomic nuclei immersed in a

Fermi sea of free neutrons, taking into account a compression of the nuclei by free neutrons (e.g., Refs. [8, 14]). For simplicity, we have used a model of free neutrons which occupy the space between atomic nuclei. At densities ρ not much higher than the neutron drip density, it is sufficiently accurate (as follows, for instance, from results of Ref. [11]). In a self-consistent approach, this model should be replaced by a more elaborated unified treatment of neutrons bound in nuclei and free outside.

In any case one should bear in mind that neutron capture reactions in a deep neutron star crust can be affected by neutron degeneracy, plasma physics, and neutron superfluidity. These effects may have important impacts on nuclear burning and nucleosynthesis in the deep neutron star crust. The effects should be taken into account to correctly simulate and interpret various observational phenomena in accreting neutron stars such as

X-ray bursts and superbursts as well as quiescent thermal emission of neutron stars in X-ray transients (e.g., Refs. [1, 2, 4] and references therein).

ACKNOWLEDGMENTS

This work is partially supported by the Joint Institute of Nuclear Astrophysics JINA (NSF-Phys-0822648). PSS and DGY acknowledge support from RFBR (grant 11-02-00253-a), RF Presidential Program NSh-4035.2012.2, and Ministry of Education and Science of Russian Federation (contract 11.G34.31.0001). PSS acknowledges support of the Dynasty Foundation. M.B. acknowledges the support from the ExtreMe Matter Institute EMMI in the framework of the Helmholtz Alliance HA216/EMMI. DGY acknowledges support of RFBR (grant 11-02-12082-ofi-m-2011).

-
- [1] T. Strohmayer and L. Bildsten, in *Compact Stellar X-Ray Sources*, edited by W. Lewin and M. van der Klis (Cambridge Univ. Press, 2006) p. 113.
 - [2] H. Schatz, L. Bildsten, and A. Cumming, *Astrophysical Journal* **583** (2003).
 - [3] A. Cumming, J. Macbeth, J. J. M. in 't Zand, and D. Page, *Astrophysical Journal* **646**, 429 (2006).
 - [4] S. Gupta, E. F. Brown, H. Schatz, P. Möller, and K.-L. Kratz, *Astrophysical Journal* **662**, 1188 (2007).
 - [5] P. Haensel and J. L. Zdunik, *Astronomy and Astrophysics* **227**, 431 (1990).
 - [6] P. Haensel and J. L. Zdunik, *Astronomy and Astrophysics* **404**, L33 (2003).
 - [7] E. F. Brown, L. Bildsten, and R. E. Rutledge, *Astrophysical Journal Letters* **504**, L95 (1998).
 - [8] P. Haensel, A. Y. Potekhin, and D. G. Yakovlev, *Neutron stars 1. Equation of state and structure* (New-York: Springer, 2007).
 - [9] S. J. Gupta, T. Kawano, and P. Möller, *Physical Review Letters* **191**, 231101 (2008).
 - [10] T. Rauscher and F.-K. Thielemann, *Atomic Data and Nuclear Data Tables* **75**, 1 (2000).
 - [11] J. W. Negele and D. Vautherin, *Nuclear Physics A* **207**, 298 (1973).
 - [12] P. S. Shternin and D. G. Yakovlev, *Physical Review D* **79**, 123004 (2009).
 - [13] A. F. Aleksandrov, L. S. Bogdankevich, and A. A. Rukhadze, *Principles of Plasma Electrodynamics*, edited by A. A. Rukhadze (Springer, New York, 1984).
 - [14] S. L. Shapiro and S. A. Teukolsky, *Black Holes, White Dwarfs, and Neutron Stars* (Wiley, New-York, 1983).
 - [15] R. H. Cyburt, A. M. Amthor, R. Ferguson, Z. Meisel, K. Smith, S. Warren, A. Heger, R. D. Hoffman, T. Rauscher, A. Sakharuk, H. Schatz, F. K. Thielemann, and M. Wiescher, *Astrophysical Journal Supplement* **189**, 240 (2010).
 - [16] A. J. Koning, S. Hilaire, and M. C. Duijvestijn, in *Proceedings of the International Conference on Nuclear Data for Science and Technology, April 22-27, 2007, Nice, France*, edited by O. Bersillon, F. Gunsing, E. Bauge, R. Jacqmin, and S. Leray (EDP Sciences, 2008) pp. 211–214.
 - [17] W. Hauser and H. Feshbach, *Physical Review* **87**, 366 (1952).
 - [18] D. Brink, *Nuclear Physics* **4**, 215 (1957).
 - [19] J. Kopecky and M. Uhl, *Phys. Rev. C* **41**, 1941 (1990).
 - [20] A. Junghans, G. Rusev, R. Schwengner, A. Wagner, and E. Grosse, *Physics Letters B* **670**, 200 (2008).
 - [21] S. Goriely, N. Chamel, and J. M. Pearson, *Phys. Rev. Lett.* **102**, 152503 (2009).
 - [22] S. Goriely, F. Tondeur, and J. Pearson, *Atomic Data and Nuclear Data Tables* **77**, 311 (2001).
 - [23] S. Goriely and E. Khan, *Nuclear Physics A* **706**, 217 (2002).
 - [24] A. Koning and J. Delaroche, *Nuclear Physics A* **713**, 231 (2003).
 - [25] J. Blakemore, *Solid State Electronics* **25**, 1067 (1982).
 - [26] G. Chabrier and A. Y. Potekhin, *Phys. Rev. E* **58**, 4941 (1998).
 - [27] X. Aymerich-Humet, F. Serra-Mestres, and J. Millán, *J. Appl. Phys.* **54**, 2850 (1983).
 - [28] G. J. Mathews, Y. Pehlivan, T. Kajino, A. B. Balantekin, and M. Kusakabe, *Astrophysical Journal* **727**, 10 (2011).
 - [29] L. R. Gasques, A. V. Afanasjev, E. F. Aguilara, M. Beard, L. C. Chamon, P. Ring, M. Wiescher, and D. G. Yakovlev, *Phys. Rev. C* **72**, 025806 (2005).
 - [30] U. Lombardo and H.-J. Schulze, in *Physics of Neutron Star Interiors*, Lecture Notes in Physics, Vol. 578, edited by D. Blaschke, N. K. Glendenning, and A. Sedrakian (Berlin: Springer Verlag, 2001) p. 30.

Appendix: Approximation of Fermi-Dirac integrals by Aymerich-Humet et al.

The asymptotes of Fermi-Dirac integrals (8) at $y \rightarrow \pm\infty$ in nondegenerate and strongly degenerate limits are easily obtained by retaining the first term in the series expansion of the Fermi-Dirac distribution function over

$\exp(x - y)$:

$$\mathcal{F}_\nu(y) = e^{-y}, \quad y \rightarrow -\infty, \quad (\text{A.1a})$$

$$\mathcal{F}_\nu(y) = \frac{y^{\nu+1}}{\Gamma(\nu+2)}, \quad y \rightarrow +\infty. \quad (\text{A.1b})$$

Aymerich-Humet et al. [27] derived a useful approximation for Fermi-Dirac integrals, which, by construction, reproduces the asymptotic limits (A.1). Their approximation reads

$$\mathcal{F}_\nu(y) = \left(\frac{\Gamma(\nu+2)2^{\nu+1}}{[b+y+(|y-b|^c+a^c)^{1/c}]^{\nu+1}} + e^{-y} \right)^{-1}, \quad (\text{A.2})$$

where the fit parameters are

$$a = \left[1 + \frac{15}{4}(\nu+1) + \frac{1}{40}(\nu+1)^2 \right]^{1/2}, \quad (\text{A.3a})$$

$$b = 1.8 + 0.61\nu, \quad (\text{A.3b})$$

$$c = 2 + (2 - \sqrt{2})2^{-\nu}. \quad (\text{A.3c})$$

In the range $-0.9 < \nu < 4$ for any y this approximation gives a relative error of $\approx 1\%$. It is also valid for larger ν but become less accurate (to about 4% at $\nu = 12$).